Open Access Journal

Journal of Power Technologies 96 (4) (2016) 306–311

journal homepage:papers.itc.pw.edu.pl

Numerical Analysis of Cavitation Phenomena with Variable Speed Centrifugal Pump

Md Rakibuzzaman[a], Kyungwuk Kim[a], Sang-Ho Suh[b,*]

[a]*Graduate School, Dept.of Mechanical Engineering, Soongsil University, Seoul, 06978, South Korea*
[b]*Department of Mechanical Engineering, Soongsil University, Seoul, 06978, South Korea*

Abstract

Cavitation is an abnormal physical phenomenon which can be generated in relatively low pressure regions in centrifugal pumps. In predicting and understanding cavitation in the pumps, it is important to secure their efficiency and reliability. The purpose of this study is to analyze the cavitation flows in centrifugal pumps with variable speeds through numerical methods. The Rayleigh–Plesset cavitation model was adapted as the source term for inter-phase mass transfer in order to predict and understand the cavitation performances. The Reynolds-average Navier-Stokes (RANS) equations were discretized by the finite volume method. The two-equation SST turbulence model was accounted for turbulent flows. The numerical analysis results were validated with experimental data and it was found that both results were in good accordance. The cavitation performances were obtained for variable speeds with different temperatures and the effects on cavitation were described according to different cavitation numbers. Cavitation performances were also observed for different centrifugal pump stages (1st and 2nd). The performances of cavitation decreased with the increase of rotational speed. In addition, the development of cavitation is elucidated according to the different temperatures, and the effects of water vapor volume fraction are discussed.

Keywords: Cavitation performance, Variable speed, Rayleigh-Plesset cavitation model, RANS equation, SST Turbulence Model

1. Introduction

Cavitation is a common physical phenomenon that plays an important role in the design and development of turbomachines such as pumps, turbines, etc. It is a process of vapor bubble formation which can be generated in relatively low pressure regions in centrifugal pumps [1]. Cavitation is a major cause of noise, vibration, erosion and performance loss in centrifugal pumps [2]. In addition, it has been found that cavitation erosion is mainly related with the length of the attached sheet cavity, the temperature of the liquid being pumped clearly affected by vapor pressure, as well as the circumferential speed and the properties of the impeller material [3]. Therefore, in order to reduce these unavoidable effects, technology for accurate prediction and understanding of cavitation is important in the development of centrifugal pumps [4].

Cavitation is also affected by the liquid temperature. Therefore, a change in temperature of the pumped liquid would affect vapor pressure and therefore the cavitation number. There is an extensive amount of literature on experimental studies conducted on different geometries (venture, hydrofoils, pumps) using diverse liquids such as refrigerants and cryogens [5, 6]. Several theoretical approaches were also made to analyze the experiment results and predict temperature effects. Investigations of thermodynamic effects have been conducted which were mainly related to the degree of temperature depression as a function of flow conditions and liquid properties. The first correlations derived by Stepanoff (1956), Moore and Ruggeri (1968, 1969) were based upon the well-known B-factor, which is defined as the ratio of vapor volume to liquid volume involved in the vaporization process [7, 8]. Kato postulated the Z-factor theory about pressure depression due to thermodynamic effects [9]. However, in spite of previous analyses, the detailed mechanism of the thermodynamic effects of cavitation has not been clearly understood.

Ruggeri and Moore measured cavitation performance in an inducer with various liquids and temperatures and suggested an empirical correlation for temperature effects on cavitation performance [10]. Franc et al. measured leading edge cavity length by visualization in an inducer at different temperatures with refrigerant R-114 as the working fluid [11]. Cervone et al. conducted experiments on the influence of water temperature on cavitation instabilities in a three blade inducer. They found that: 1) the intensity of cavitation surge was weaker at higher temperatures (343K)

*Corresponding author
Email address: suhsh@ssu.ac.kr (Sang-Ho Suh)

than at lower temperatures (297K) and 2) increasing temperature did not change either frequency or type of cavitation instabilities [12]. Torre et al. found that the critical cavitation number was higher when the water temperature was lower [13]. However, they did not show a clear relationship between the critical cavitation number and water temperatures, and how temperature change was affected by the variable speeds.

The present study is focused on investigating cavitation performances and variable speed changes in centrifugal pumps numerically. Also, the development of cavitation is described according to different temperatures. In the numerical prediction, the R-P cavitation model and two-phase homogeneous liquid-vapor methods were used. The governing equations were discretized by finite volume methods. The cavitation number curves were estimated from the head coefficient drop lines for variable speeds for different flows.

2. Numerical Method

In the numerical analysis, the fluid in the pump field was considered as a homogeneous, incompressible mixed medium of vapor and liquid. The governing differential equations are given as Eq. (1), (2);

$$\frac{\partial \rho_m}{\partial t} + \frac{\partial (\rho_m u_j)}{\partial x_j} = 0 \tag{1}$$

$$\rho_m \left(\frac{\partial u_i}{\partial t} + u_j \frac{\partial u_i}{\partial x_j} \right) = -\frac{\partial p}{\partial x_i} + \frac{\partial}{\partial x_j} \left[(\mu_m + \mu_t) \left(\frac{\partial u_i}{\partial x_j} + \frac{\partial u_j}{\partial x_i} \right) \right] \tag{2}$$

where ρ_m and μ_m are the mixture density and dynamic viscosity, calculated by the weighted average of each phase volume fraction, u_i is the velocity, and μ_t is the turbulent viscosity, respectively.
The mixture density and turbulence viscosity are defined by Eq. (3):

$$\begin{aligned} \rho_m &= \rho_l \alpha_l + \rho_v (1-\alpha_l) \\ \mu_m &= \mu_l \alpha_l + \mu_v (1-\alpha_l) \end{aligned} \tag{3}$$

The sum of all volume fractions must equal one.

$$\alpha_l + \alpha_g + \alpha_v = 1 \tag{4}$$

The volume fractions were related to the mass fractions, f, for each component through the following relations as Eq. (5):

$$f_g = \frac{\alpha_g \rho_g}{\rho_m}, f_v = \frac{\alpha_v \rho_v}{\rho_m}, f_l = \frac{\alpha_l \rho_l}{\rho_m} = 1 - f_v - f_g \tag{5}$$

where f_v, f_g, f_l are the component mass fraction of the vapor, gas, and liquid; ρ_v, ρ_g, ρ_l are the component densities, α_v, α_g, α_l are the component of volume fractions. The liquid-vapor transfer due to cavitation was modeled by a vapor volume fraction transport equation expressed as Eq. (6):

$$\frac{\partial}{\partial t}(\rho_m \alpha_m) + \frac{\partial}{\partial t}(\rho_m \alpha_m u_j) = \dot{S}_l \tag{6}$$

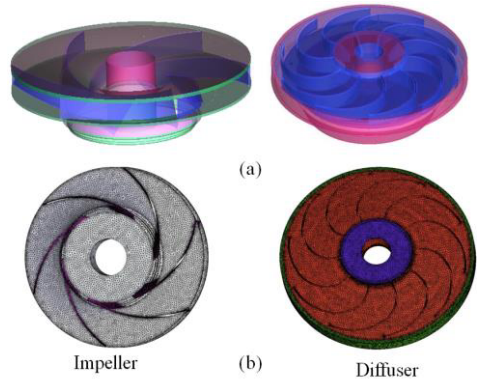

Figure 1: Geometrical model and unconstructed meshing of the pump

Table 1: Pump impeller design specification

Design flow rate	Rotation speed	Blade number	Impeller diameter	Outlet width
Q m^3/hr	N rev/min	Z	D_2 m	b_2 m
24	3,600	6	0.1047	0.008

where $\alpha_v = 1 - \alpha_m$, and $\dot{S}_l = -\dot{S}_v$.
The source terms have units of (kg/s) where the source terms $\dot{S}_v$ and $\dot{S}_l$ account for mass exchange (evaporation and condensation) between the vapor and liquid in the primary phases during cavitation. The formation and collapse of a cavity was modeled as a phase transformation. A cavitation model was used, based on the Rayleigh-Plesset equation (R-P) to estimate the rate of vapor production [14]. Neglecting the second order term and surface tension force, the R-P equation is simplified to Eq. (7):

$$\frac{dR_B}{dt} = \sqrt{\frac{2}{3} \frac{|p_v - p|}{\rho_l}} \tag{7}$$

This equation provided a physical method to incorporate the influence of bubble dynamics into the cavitation model. The evaporation and conduction rate can be expressed as Eq. (8):

$$\begin{aligned} \dot{S}_v &= F_{vap} \frac{3\alpha_{nuc}(1-\alpha_v)}{R_B} \rho_v \sqrt{\frac{2}{3} \frac{|p_v - p|}{\rho_l}} \, \mathrm{sgn}(p_v - p) \\ \dot{S}_l &= -F_{cond} \frac{3\alpha_v}{R_B} \rho_v \sqrt{\frac{2}{3} \frac{|p_v - p|}{\rho_l}} \, \mathrm{sgn}(p_v - p) \end{aligned} \tag{8}$$

where α_{nuc} is the nucleation site volume fraction at 5.0×10^{-4}, R_B is the radius of a nucleation site at 1.0×10^{-6} m. The recommended values of the empirical parameters F_{vap} and F_{cond} are 50 and 0.01 for evaporation and condensation, respectively; if $p < p_v$ evaporation occurs and if $p > p_v$ condensation occurs.

3. Computational Analysis

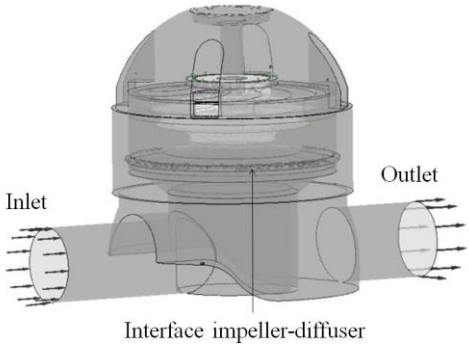

Figure 2: Interface domain of the impeller-diffuser

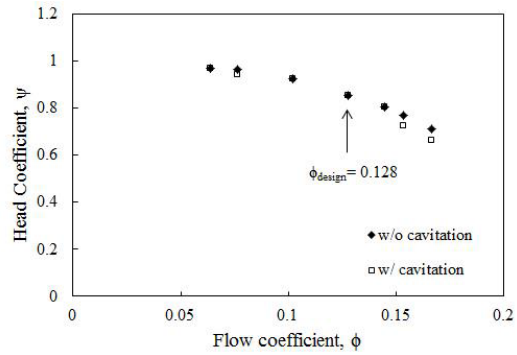

Figure 3: Computed head coefficient versus flow coefficient for without and with cavitation

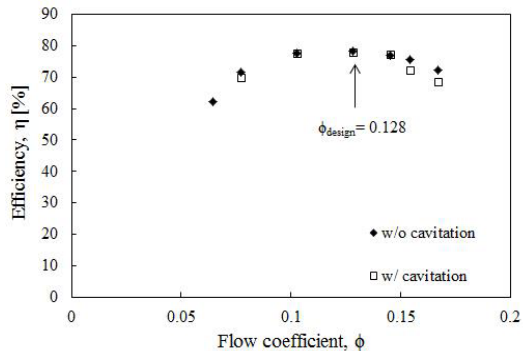

Figure 4: Computed efficiency versus flow coefficient for without and with cavitation

The model pump was used for the first and second stages in cavitation conditions. Fig. 1(a) shows the impeller and diffuser of the model pump. The model pump was meshed by ANSYS ICEM-CFX (Ansys Inc. 2013, USA), based on finite volume methods (FVM) [15]. The pump model impeller, diffuser, and casing were meshed and a mesh dependency test (impeller and diffuser) was performed under non-cavitating conditions at a design operating flow (24 m^3/hr) and it was found that the pressure drop error was less than 1%. The total meshed element and nodes were 4,477,248 and 1,417,827. The unconstructed tetra-prim meshing of the centrifugal pump is shown in Fig. 1(b). Under the cavitation condition, the impeller domain was rotating on a z-axis at variable speeds with different flow operating conditions, and the diffuser was on a stationary domain. A frozen rotor was applied to couple the rotation and stationary domain. The impeller-diffuser of the pump domain is shown in Fig. 2. The inlet boundary's total pressure and mass flow rate was imposed at the outlet boundary. All boundary walls were assumed as smooth walls with non-slip conditions. The frozen rotor simulation was selected for the steady state analysis at a given rotational speed. Also, different temperatures were considered for different vapor pressures. The SST turbulence model [15, 16] was used to solve the turbulence phenomena of the fluid. High resolution for the advection scheme, first order for the turbulence numeric and SIMPLEC algorithms were considered in the solver control. The residual value was 1×10^{-5} controlled by convergence criteria. Table 1 shows the design specification of the centrifugal pump model for the simulations.

4. Results and Discussion

In what follows, four parameters were used to define the operating point and performance of the pump. These were head coefficient, flow coefficient, cavitation number, and efficiency; which are defined respectively here as:

$$\psi = \frac{2gH}{U_{tip}^2} \tag{9}$$

$$\phi = \frac{Q}{\pi D_2 b_2 U_{tip}} \tag{10}$$

$$\sigma = \frac{p_{in} - p_v}{0.5\rho_l U_{tip}^2} \tag{11}$$

$$\eta = \frac{\rho Q g H}{\omega T} \tag{12}$$

Computational performances are presented in Fig. 3, without (single phase) cavitation and with (two-phase) cavitation computational performances are presented. The plotted graph represents head coefficient versus flow coefficient. The figure shows that a small deviation occurred between without and with cavitation. Flow stability occurred just before and after the design flow coefficient. Also, it was noticed that with the increased flow coefficient after design flow, head deterioration was reached and void of fraction might have appeared and formed on the impeller blade and degraded performances.

Fig. 4 shows hydraulic efficiency versus flow coefficient for a range of flow coefficients, $0.077 \leq \phi_{design} \leq 0.167$. For each flow coefficient, without cavitation and with cavitation calculations were performed.

Fig. 5 shows a comparison of experimental and a computed head–coefficient versus cavitation number. It is seen that the comparison of results were in good agreement.

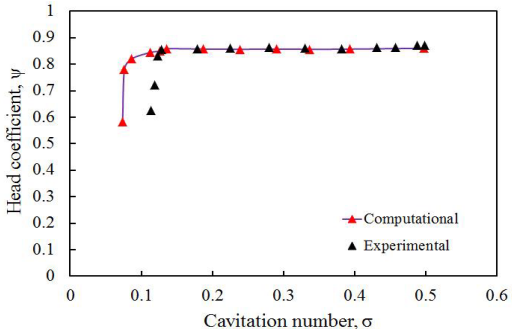

Figure 5: Comparison between predicted and experiment results at design flow rate

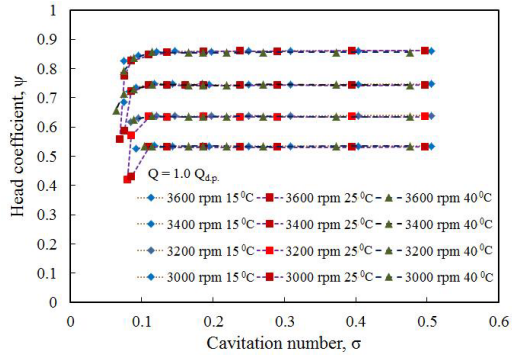

Figure 6: Pump cavitation performance at nominal flow coefficient, temperatures, and rotational speeds of 3000 rpm, 3200 rpm, 3400 rpm and 3600 rpm

4.1. Cavitation performance for variable speeds

Cavitation performance is presented in Fig. 6 at a rotational speed of 3600 rpm, 3400 rpm, 3200 rpm, and 3000 rpm at three different temperatures, $15°C$, $25°C$, $40°C$ (288, 298 and 313K). The reference fluid temperature was considered $25°C$ (298K). The pump head-coefficient ratio is shown in Fig. 6 as a function of the required cavitation number for the design flow rate ($Q_{d.p.}$). The head-coefficient drop lines were obtained by reducing impeller suction. From Fig. 6, it is noticeable that the initial decrease of the cavitation number had no effect on the head-coefficient drop curves because the pump and head-coefficient remained unchanged. As the cavitation number decreased, the head-coefficient decreased and dropped sharply at lower cavitation numbers. The head drop varied for different rotational speeds at different water temperatures. At a design rotational speed of 3600 rpm, the head-coefficient was constant and dropped steeply at a value of $\sigma = 0.136$. When the rotational speed was gradually decreased the head-coefficient started to drop before the design rotational speed of 3600 rpm. At 3400 rpm the head-coefficient started to drop to $\sigma = 0.162$, which was larger than at 3600 rpm. At 3200 rpm it began to drop to $\sigma = 0.136$ which was similar with the design rotational speed. At 3000 rpm the total head degraded and dropped to $\sigma = 0.147$. In the end, the head-coefficient dropped sharply and the full cavitation or head breakdown occurred completely.

On the other hand, it was noticed from the figure that with increasing temperature, the head-coefficient drops from a lower cavitation number to a higher cavitation number for different variable speeds.

The contours of the computed vapor volume fraction on the meridional view of the impeller blades at a variation speed of 3000 rpm, 3200 rpm, 3400 rpm, and 3600 rpm are shown in Fig.7 at a design flow rate.

The vapor volume fraction contours is from 0-1. From this figure, it is noticeable that the development of cavitation changes with different rotational speeds. For $\sigma = 0.187$, the propagation of cavitation was started from the suction shroud leading edge. The length of the attached cavity was increased from the suction shroud to the hub side. At 3000 rpm, the development of attached cavitation was affected less at the suction shroud than at 3600 rpm. With the decreasing cavitation number ($\sigma = 0.136$), visual observation indicated that the attached cavitation extension gradually increased as the rotational speed increased. An initial head-coefficient drop occurred when vortex cavitation almost covered the throat region of the flow passage.

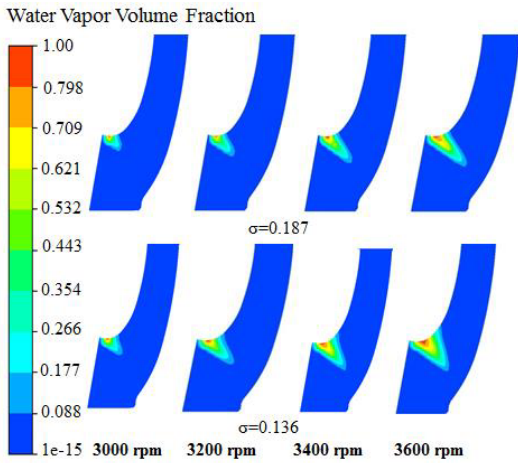

Figure 7: Cavitation performance effect at four different rotational three speeds (Flow coefficient = 0.128, water temperature = $25°C$)

Fig. 8 shows the head coefficient drop curve as a function of cavitation number for different pump stages (1st and 2nd stage). The circle represents a three percent head-coefficient drop in the head drop line. It was observed from the cavitation performance curve that a 3% head drop occurred at the same cavitation number.

4.2. Temperature effects

The change in temperature of the pumped liquid would affect the vapor pressure and cavitation number. Therefore, the temperature effect that relates to the mechanism of heat and interface mass transfer is associated with cavitation. Fig. 9 shows the head coefficient drop curves for water pumped at four different temperatures ($15°C$, $25°C$, $40°C$ and $50°C$) for three different flow rates. The figures show that

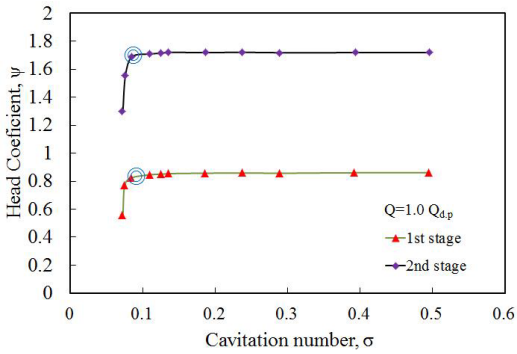

Figure 8: Head coefficient versus cavitation number for different pump stage

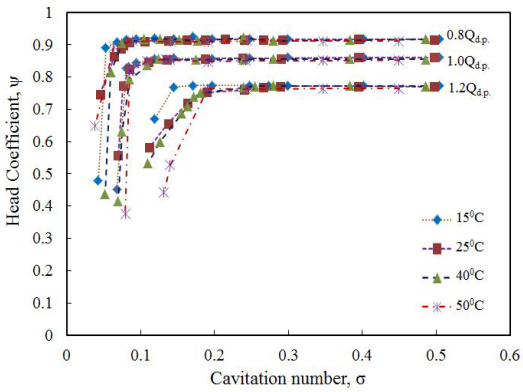

Figure 9: Computed cavitation performance characteristics at three nominal flow co-efficients, temperatures (15°C, 25°C, 40°C, 50°C) and rotational speed of 3600 rpm

pumping high temperature water requires a high cavitation number.

As can be seen from the figure, cavitation breakdown increases substantially with increasing temperatures. At the design flow rate ($Q = 1.0\,Q_{d.p}$) the head drops steeply at lower cavitation numbers for various water temperatures but for the highest water temperature it drops earlier than the other three different temperatures (15°C, 25°C and 40°C).

In the end, the head drops gradually decreased or head breakdown occurred. Therefore, liquid-vapor phase flow prevails in the large portion of the impeller blades. At lower temperatures, cavitation occurred at lower cavitation numbers, but at higher temperatures, it occurred at higher cavitation numbers. This means that at higher temperatures, cavitation erosion on the impeller blade might occur more quickly than at lower temperatures.

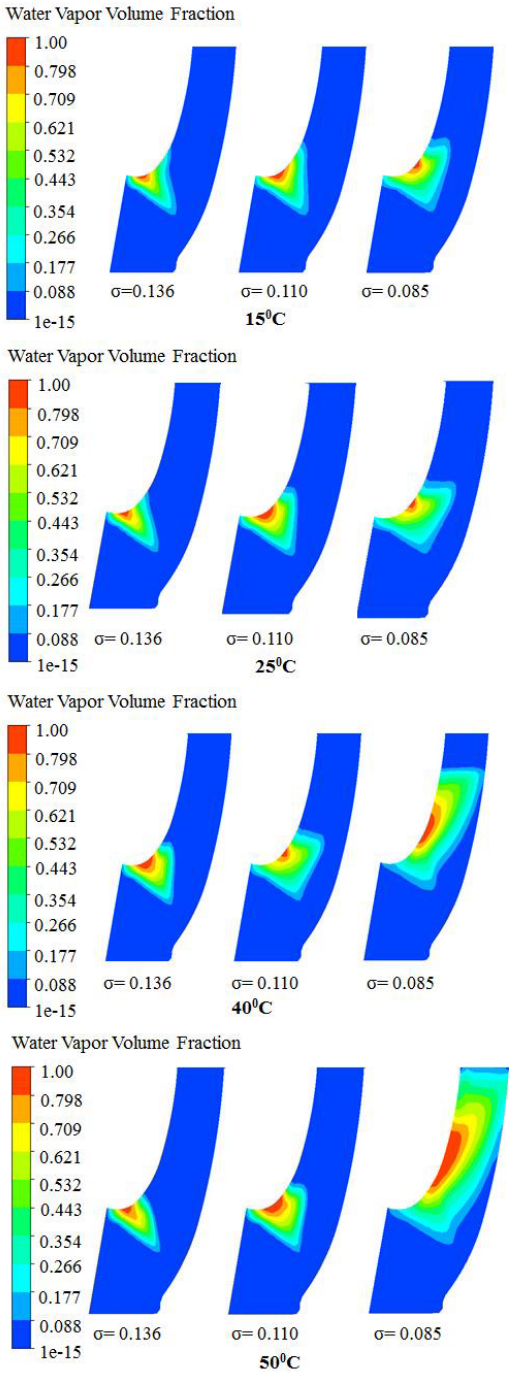

Figure 10: Computed cavitation performance characteristics at three nominal flow co-efficients, temperatures (15°C, 25°C, 40°C, 50°C) and rotational speed of 3600 rpm

This thermal effect can be extended to attached or blade cavities with changes in detail as shown in Fig. 10. Fig. 10 shows the cavitation development effect in the meridional view on the impeller blade at four different temperatures with different cavitation numbers at the design flow rate. It was implied that at $\sigma = 0.136$ the development of attached cavitation was almost the same for the four various temperatures (15°C, 25°C, 40°C and 50°C) but for the $\sigma = 0.110$, the development of cavitation was less effected at 15°C than

the others; and at $40°C$ and $50°C$, the region of cavitation was increased from the shroud to the hub side. Finally for $\sigma = 0.085$, full cavitation or complete head breakdown occurred at $40°C$ and $50°C$, which caused the complete obstruction that of the blade cavity region, blocking the internal circulation flow of the model pump.

5. Conclusion

A Rayleigh–Plesset cavitation model was used to simulate the ANSYS-CFX code. Steady simulations were performed with a shear stress transport turbulence model to perform the cavitation phenomena at variable speeds with different flow operating conditions. The head coefficient curves were obtained for variable angular speeds and the performances were described according to the cavitation number. Also, the developments of attached cavitation performances were estimated and described by the temperature effects. The propagation of cavitation on the impeller blade from the suction leading edge to the trailing edge was observed. The results show that attached cavitation can directly lead to losses in efficiency, especially for flow rates inside the cavitation zone. Cavitation formation happened more quickly at higher temperatures than at lower temperatures.

Acknowledgements

This work was supported by the Korea institute of Energy Technology Evaluation and Planning (KETEP). The grant number is 20132010101870 for the Promotion of Science.

References

[1] B. Schiavello, F. C. Visser, Pump cavitation—various npshr criteria, npsha margins, and impeller life expectancy, in: Proceedings of the 25th International Pump Users Symposium, Turbomachinery Laboratory, Texas A&M University, College Station, TX, 2009, pp. 113–144.
[2] Japan Association of Agriculture Engineering Enterprises, Pumping Station Engineering Hand Book, Tokyo, (1991), pp. 50-90.
[3] C. E. Brennen, Hydrodynamics of pump, Oxford University Press, 1994.
[4] B. R. Shin, et, al., Application of preconditioning method to gas-liquid two-phase flow computations, Journal of Fluids Engineering, ASME 126 (2004) 605–612.
[5] Hord J., Cavitation in liquid cryogens, Vol. I II III & IV NASA CR-2054/2156/2242/2448 (1972a, 1972b, 1973, 1974).
[6] G. Kovich, Comparison of predicted and experimental cavitation performance of 84 helical inducer in water and hydrogen, Vol. 7016, National Aeronautics and Space Administration, 1970.
[7] H. A. Stahl, A. J. Stepanoff, N. Phillipsburg, Thermodynamic aspects of cavitation in centrifugal pumps, ASME J. Basic Eng 78 (1956) 1691–1693.
[8] Moore R.D. & Ruggeri R.S., Prediction of thermodynamic effects of developed cavitation based on liquid hydrogen and freon-114 data in scaled venturis, NASA TN D-4899, 1968.
[9] H. Kato, H. Yamaguchi, S. Okada, K. Kikuchi, M. Myanaga, Thermodynamic effect on incipient and developed sheet cavitation, in: International Symposium on Cavitation Inception, 1984, pp. 127–136.
[10] R. S. Ruggeri, R. D. Moore, Method for prediction of pump cavitation performance for various liquids, liquid temperatures, and rotative speeds, National Aeronautics and Space Administration, 1969.
[11] J.-P. Franc, E. Janson, P. Morel, C. Rebattet, M. Riondet, Visualizations of leading edge cavitation in an inducer at different temperatures, 4th International Symposium on Cavitation, CAV2001, Pasadena, CA, June 20–23, 2001.
[12] A. Cervone, R. Testa, C. Bramanti, E. Rapposelli, L. D'Agostino, Thermal effects on cavitation instabilities in helical inducers, Journal of propulsion and power 21 (5) (2005) 893–899.
[13] L. Torre, A. Cervone, A. Pasini, L. d'Agostino, Experimental characterization of thermal cavitation effects on space rocket axial inducers, Journal of Fluids Engineering 133 (11) (2011) 111303.
[14] F. Bakir, R. Rey, A. Gerber, T. Belamri, B. Hutchinson, Numerical and experimental investigations of the cavitating behavior of an inducer, International Journal of Rotating Machinery 10 (1) (2004) 15–25.
[15] N. J. Georgiadis, D. A. Yoder, W. B. Engblom, Evaluation of modified two-equation turbulence models for jet flow predictions, AIAA journal 44 (12) (2006) 3107–3114.
[16] Ansys Inc. 2013, ANSYS-CFX (CFX Introduction, CFX Reference guide, CFX Tutorials, CFX-Pre User's Guide, CFX-Solver Manager User's Guide, Theory Guide), release 14.5, USA.

Nomenclature

Parameters

g	Acceleration due to gravity [m/s^2]
U_{tip}	Blade tip speed [m/s]
σ	Cavitation number [-]
ψ	Head coefficient [-]
ϕ	Flow coefficient [-]
ω	Angular velocity [rad/s]
T	Torque [N·m]
α	Volume fraction
μ	Viscosity [Pa·s]

Subscripts

i,j	tensor indices
l	liquid
m	mixture
g	gas
$1,2$	inlet, exit